Miloslav Feistauer; Vít Dolejší

Discontinuous Galerkin method for compressible flow and conservation laws

In: Jan Chleboun and Petr Přikryl and Karel Segeth (eds.): Programs and Algorithms of Numerical Mathematics, Proceedings of Seminar. Dolní Maxov, June 6-11, 2004. Institute of Mathematics AS CR, Prague, 2004. pp. 47–62.

Persistent URL: http://dml.cz/dmlcz/702775

DISCONTINUOUS GALERKIN METHOD FOR COMPRESSIBLE FLOW AND CONSERVATION LAWS *

Miloslav Feistauer, Vít Dolejší

Abstract

This paper is concerned with the application of the discontinuous Galerkin finite element method to the numerical solution of the compressible Navier-Stokes equations. The attention is paid to the derivation of discontinuous Galerkin finite element schemes and to the investigation of the accuracy of the symmetric as well as nonsymmetric discretization.

1. Introduction

In the numerical solution of elliptic or parabolic problems, usually conforming (i.e. continuous) finite element approximations are used. However, singularly perturbed problems or nonlinear conservation laws of fluid dynamics have solutions with steep gradients or discontinuities and their approximations by conforming finite elements suffer from the Gibbs phenomenon. One way how to avoid this drawback is to use a suitable stabilization as, e.g. the streamline diffusion method or Galerkin least squares method and shock capturing stabilization.

On the other hand, there is a question, if it is not suitable to relax the continuity of finite element approximations of discontinuous solutions to conservation laws, similarly as in the finite volume methods. The use of advantages of the finite volume and finite element techniques leads to the *discontinuous Galerkin finite element method* (DGFEM). This technique is based on the idea to approximate the solution of an initial-boundary value problem by piecewise polynomial functions over a finite element mesh without any requirement on interelement continuity. The DGFEM was applied to nonlinear conservation laws already in 1989 by Cockburn and Shu ([9]). It was used for the numerical simulation of compressible flow later by Bassi and Rebay in [2] and [3]. During several recent years the DGFE schemes have been extensively developed and become more and more popular. Some aspects of the DGFEM and applications to gas dynamics are also discussed in [1], [15], [16], [17], [11], [12]. For a survey, see e. g. [7] and [8].

In this paper we are concerned with the application of the discontinuous Galerkin finite element method to the compressible Navier-Stokes equations. First, we pay the attention to the derivation of DGFE schemes and give examples of the solution of viscous compressible flow. Then we investigate the accuracy of the DGFEM on

*This work was supported by Grant No. 201/05/0005 of the Grant Agency of the Czech Republic and Grant No. MSM 0021620839 of the Ministry of Education of the Czech Republic.

a model scalar convection-diffusion equation. We discuss two ways of the discretization of diffusion terms (symmetric and nonsymmetric), mention some theoretical results and present the verification of the accuracy of the method with the aid of numerical experiments.

2. DGFEM for compressible flow

In this section we describe the application of the DGFEM to the numerical solution of viscous compressible flow.

2.1. Governing equations

Let $\Omega \subset \mathbb{R}^d$ $(d = 2, 3)$ be a bounded domain occupied by gas, and $T > 0$. We set $Q_T = \Omega \times (0, T)$ and by $\partial\Omega$ we denote the boundary of Ω which consists of several disjoint parts. We distinguish inlet Γ_I, outlet Γ_O and impermeable walls Γ_W on $\partial\Omega$. We want to find a vector-valued function $\boldsymbol{w} : Q_T \to \mathbb{R}^m,\ m = d + 2$, such that

$$\frac{\partial \boldsymbol{w}}{\partial t} + \sum_{s=1}^{d} \frac{\partial \boldsymbol{f}_s(\boldsymbol{w})}{\partial x_s} = \sum_{s=1}^{d} \frac{\partial \boldsymbol{R}_s(\boldsymbol{w}, \nabla \boldsymbol{w})}{\partial x_s} \quad \text{in } Q_T, \tag{1}$$

where $Q_T = \Omega \times (0, T)$ and

$$\begin{aligned}
\boldsymbol{w} &= (\rho, \rho v_1, \dots, \rho v_d, E)^{\mathrm{T}} \in \mathbb{R}^m, \\
\boldsymbol{w} &= \boldsymbol{w}(x, t),\ x \in \Omega,\ t \in (0, T), \\
\boldsymbol{f}_i(\boldsymbol{w}) &= (f_{i1}, \dots, f_{im})^{\mathrm{T}} \\
&= (\rho v_i, \rho v_1 v_i + \delta_{1i}\, p, \dots, \rho v_d v_i + \delta_{di}\, p, (E + p) v_i)^{\mathrm{T}} \\
\boldsymbol{R}_i(\boldsymbol{w}, \nabla \boldsymbol{w}) &= (R_{i1}, \dots, R_{im})^{\mathrm{T}} \\
&= (0, \tau_{i1}, \dots, \tau_{id}, \tau_{i1}\, v_1 + \dots + \tau_{id}\, v_d + k \partial\theta/\partial x_i)^{\mathrm{T}}, \\
\tau_{ij} &= \lambda \operatorname{div} \boldsymbol{v} \delta_{ij} + \mu \left(\frac{\partial v_i}{\partial x_j} + \frac{\partial v_j}{\partial x_i} \right),
\end{aligned} \tag{2}$$

The symbol $\nabla \boldsymbol{w}$ denotes the gradient of $\boldsymbol{w}$. To system (1) we add the thermodynamical relations

$$p = (\gamma - 1)(E - \rho |\boldsymbol{v}|^2/2), \quad \theta = \left(\frac{E}{\rho} - \frac{1}{2} |\boldsymbol{v}|^2 \right) / c_v. \tag{3}$$

We use the following *notation*: $\boldsymbol{v} = (v_1, \dots, v_d)^{\mathrm{T}}$ – velocity vector, ρ – density, p – pressure, θ – absolute temperature, E – total energy, γ – Poisson adiabatic constant, c_v – specific heat at constant volume, μ, λ – viscosity coefficients, k – heat conduction coefficient, δ_{ij} – Kronecker symbol. We assume that γ, c_v, μ, k are constants and $\mu, k, c_v > 0$, $2\mu + 3\lambda \geq 0$. Usually we set $\lambda = -2\mu/3$.

System (1) is equipped with the initial condition

$$\boldsymbol{w}(x,0) = \boldsymbol{w}^0(x), \quad x \in \Omega, \tag{4}$$

and the following boundary conditions on appropriate parts of the boundary:

$$\begin{aligned} &\text{a)}\ \ \rho|_{\Gamma_I\times(0,T)} = \rho_D, \quad \text{b)}\ \ \boldsymbol{v}|_{\Gamma_I\times(0,T)} = \boldsymbol{v}_D = (v_{D1},\dots,v_{Dd})^{\mathrm{T}}, \\ &\text{c)}\ \ \theta|_{\Gamma_I} = \theta_D \quad \text{on } \Gamma_I\times(0,T); \end{aligned} \tag{5}$$

$$\text{a)}\ \ \boldsymbol{v}|_{\Gamma_W\times(0,T)} = 0, \quad \text{b)}\ \ \frac{\partial\theta}{\partial n}|_{\Gamma_W\times(0,T)} = 0 \quad \text{on } \Gamma_W\times(0,T); \tag{6}$$

$$\text{a)}\ \sum_{i=1}^{d}\tau_{ij}n_i = 0, \quad j=1,\dots,d, \quad \frac{\partial\theta}{\partial n} = 0 \quad \text{on } \Gamma_O\times(0,T). \tag{7}$$

The problem to solve the compressible Navier-Stokes equations, equipped with the above initial and boundary conditions will be denoted by (CFP) (compressible flow problem).

2.2. Discretization

By Ω_h we denote a polygonal or polyhedral approximation of the domain Ω, if $d=2$ or $d=3$, respectively. Let $\mathcal{T}_h$ $(h>0)$ denote a partition of the closure $\overline{\Omega}_h$ of the domain Ω_h into a finite number of closed convex polygons (if $d=2$) or polyhedra (if $d=3$) K with mutually disjoint interiors. We call $\mathcal{T}_h$ a triangulation of Ω_h, but *do not* require the usual conforming properties from the finite element method. In 2D problems we usually choose $K\in\mathcal{T}_h$ as triangles or quadrilaterals, in 3D, $K\in\mathcal{T}_h$ can be, e.g., tetrahedra, pyramids or hexahedra, but we can allow even more general elements K.

We set $h_K = \operatorname{diam}(K)$, $h = \max_{K\in\mathcal{T}_h} h_K$. By $|K|$ we denote the d-dimensional Lebesgue measure of K. All elements of $\mathcal{T}_h$ will be numbered so that $\mathcal{T}_h = \{K_i\}_{i\in I}$, where $I\subset Z^+ = \{0,1,2,\dots\}$ is a suitable index set. If two elements K_i, $K_j\in\mathcal{T}_h$ contain a nonempty open face, we call them *neighbours*. We set in this case $\Gamma_{ij} = \partial K_i\cap\partial K_j$. For $i\in I$ we set $s(i) = \{j\in I; K_j \text{ is a neighbour of } K_i\}$. The boundary $\partial\Omega_h$ is formed by a finite number of faces of elements K_i adjacent to $\partial\Omega_h$. We denote all these boundary faces by S_j, where $j\in I_b\subset Z^- = \{-1,-2,\dots\}$, and set $\gamma(i) = \{j\in I_b; S_j \text{ is a face of } K_i\}, \Gamma_{ij} = S_j$ for $K_i\in\mathcal{T}_h$ such that $S_j\subset\partial K_i$, $j\in I_b$. For K_i not containing any boundary face S_j we set $\gamma(i)=\emptyset$. Obviously, $s(i)\cap\gamma(i)=\emptyset$ for all $i\in I$. Now, if we write $S(i) = s(i)\cup\gamma(i)$, we have

$$\partial K_i = \bigcup_{j\in S(i)}\Gamma_{ij}, \qquad \partial K_i\cap\partial\Omega_h = \bigcup_{j\in\gamma(i)}\Gamma_{ij}. \tag{8}$$

Furthermore, we use the following notation: $\boldsymbol{n}_{ij} = ((n_{ij})_1,\dots,(n_{ij})_d)$ = unit outer normal to ∂K_i on the face Γ_{ij}, $d(\Gamma_{ij}) = \operatorname{diam}(\Gamma_{ij}), |\Gamma_{ij}| = (d-1)$-dimensional Lebesgue measure of Γ_{ij}.

Over the triangulation $\mathcal{T}_h$ we define the *broken Sobolev space*

$$H^k(\Omega, \mathcal{T}_h) = \{v; v|_K \in H^k(K) \ \forall\, K \in \mathcal{T}_h\}. \tag{9}$$

For $v \in H^1(\Omega, \mathcal{T}_h)$ we set

$$\begin{aligned} v|_{\Gamma_{ij}} = \text{ trace of } v|_{K_i} \text{ on } \Gamma_{ij}, \quad v|_{\Gamma_{ji}} = \text{ trace of } v|_{K_j} \text{ on } \Gamma_{ij}, \quad i \in I,\ j \in S(i), \\ \langle v \rangle_{\Gamma_{ij}} = \frac{1}{2}\left(v|_{\Gamma_{ij}} + v|_{\Gamma_{ji}}\right) \quad \text{and} \quad [v]_{\Gamma_{ij}} = v|_{\Gamma_{ij}} - v|_{\Gamma_{ji}},\ i \in I, \quad j \in s(i), \end{aligned} \tag{10}$$

denoting the *traces, average* and *jump of the traces* of v on $\Gamma_{ij} = \Gamma_{ji}$, respectively. Obviously, $\langle v \rangle_{\Gamma_{ij}} = \langle v \rangle_{\Gamma_{ji}}$, $[v]_{\Gamma_{ij}} = -[v]_{\Gamma_{ji}}$ and $[v]_{\Gamma_{ij}} \boldsymbol{n}_{ij} = [v]_{\Gamma_{ji}} \boldsymbol{n}_{ji}$.

Let us define the finite dimensional space

$$S_h = S^{p,-1}(\Omega, \mathcal{T}_h) = \{v; v|_K \in P^p(K) \ \forall\, K \in \mathcal{T}_h\}, \tag{11}$$

where $p \geq 1$ is an integer and $P^p(K)$ denotes the space of all polynomials on K of degree $\leq p$.

The approximate solution $\boldsymbol{w}_h$ as well as test functions $\boldsymbol{\varphi}_h$ are elements of the finite dimensional space of vector-valued functions

$$\boldsymbol{S}_h = [S_h]^m. \tag{12}$$

By $\gamma_D(i)$ we denote the subset of such indexes $j \in \gamma(i)$ that for at least one component w_r of the sought solution $\boldsymbol{w}$ the Dirichlet condition is prescribed on the part of $\partial\Omega$ approximated by the face $\Gamma_{ij} \subset \partial\Omega_h$.

Now let us derive the discrete problem. For a while we assume that $\Omega_h = \Omega$. Assuming that $\boldsymbol{w}$ is a classical sufficiently regular solution of problem (CFP) and $\boldsymbol{\varphi} \in H^2(\Omega, \mathcal{T}_h)^m$, we multiply equation (1) by $\boldsymbol{\varphi}$, integrate over $K_i \in \mathcal{T}_h$, apply Green's theorem, sum over all $K_i \in \mathcal{T}_h$, use conditions (6), b) and (7) and arrive at the identity

$$\begin{aligned} &\int_{\Omega_h} \frac{\partial \boldsymbol{w}}{\partial t} \cdot \boldsymbol{\varphi}\, dx + \sum_{i \in I} \sum_{j \in S(i)} \int_{\Gamma_{ij}} \sum_{s=1}^{d} \boldsymbol{f}_s(\boldsymbol{w})\, (n_{ij})_s \cdot \boldsymbol{\varphi}|_{\Gamma_{ij}} dS \\ &- \sum_{i \in I} \int_{K_i} \sum_{s=1}^{d} \boldsymbol{f}_s(\boldsymbol{w}) \cdot \frac{\partial \boldsymbol{\varphi}}{\partial x_s}\, dx + \sum_{i \in I} \int_{K_i} \sum_{s=1}^{d} \boldsymbol{R}_s(\boldsymbol{w}, \nabla \boldsymbol{w}) \cdot \frac{\partial \boldsymbol{\varphi}}{\partial x_s}\, dx \\ &- \sum_{i \in I} \sum_{\substack{j \in s(i) \\ j<i}} \int_{\Gamma_{ij}} \sum_{s=1}^{d} \langle \boldsymbol{R}_s(\boldsymbol{w}, \nabla \boldsymbol{w}) \rangle\, (n_{ij})_s \cdot [\boldsymbol{\varphi}]\, dS \\ &- \sum_{i \in I} \sum_{j \in \gamma_D(i)} \int_{\Gamma_{ij}} \sum_{s=1}^{d} \boldsymbol{R}_s(\boldsymbol{w}, \nabla \boldsymbol{w})\, (n_{ij})_s \cdot \boldsymbol{\varphi}\, dS = 0, \end{aligned} \tag{13}$$

which is the basis for the derivation of the DGFE scheme. It is necessary to introduce in (13) suitable stabilization terms. To this end, we carry out a partial linearization

of viscous fluxes $\boldsymbol{R}_s$. We expess them in terms of variables $w_1, \ldots, w_m$ and their derivatives.

For example, for $d = 2$ and $\lambda = -2\mu/3$, from (2) we obtain

$$\boldsymbol{R}_1(\boldsymbol{w}, \nabla \boldsymbol{w}) \tag{14}$$

$$= \begin{pmatrix} 0 \\ \frac{2}{3}\,\frac{\mu}{w_1}\left[2\left(\frac{\partial w_2}{\partial x_1} - \frac{w_2}{w_1}\,\frac{\partial w_1}{\partial x_1}\right) - \left(\frac{\partial w_3}{\partial x_2} - \frac{w_3}{w_1}\,\frac{\partial w_1}{\partial x_2}\right)\right] \\ \frac{\mu}{w_1}\left[\left(\frac{\partial w_3}{\partial x_1} - \frac{w_3}{w_1}\,\frac{\partial w_1}{\partial x_1}\right) + \left(\frac{\partial w_2}{\partial x_2} - \frac{w_2}{w_1}\,\frac{\partial w_1}{\partial x_2}\right)\right] \\ \frac{w_2}{w_1}\,\boldsymbol{R}_1^{(2)} + \frac{w_3}{w_1}\,\boldsymbol{R}_1^{(3)} + \frac{k}{c_v w_1}\Big[\frac{\partial w_4}{\partial x_1} - \frac{w_4}{w_1}\,\frac{\partial w_1}{\partial x_1} - \frac{1}{w_1}\left(w_2\,\frac{\partial w_2}{\partial x_1} + w_3\,\frac{\partial w_3}{\partial x_1}\right) \\ \qquad\qquad + \frac{1}{w_1^2}\,(w_2^2 + w_3^2)\,\frac{\partial w_1}{\partial x_1}\ \Big] \end{pmatrix},$$

$$\boldsymbol{R}_2(\boldsymbol{w}, \nabla \boldsymbol{w})$$

$$= \begin{pmatrix} 0 \\ \frac{\mu}{w_1}\left[\left(\frac{\partial w_3}{\partial x_1} - \frac{w_3}{w_1}\,\frac{\partial w_1}{\partial x_1}\right) + \left(\frac{\partial w_2}{\partial x_2} - \frac{w_2}{w_1}\,\frac{\partial w_1}{\partial x_2}\right)\right] \\ \frac{2}{3}\,\frac{\mu}{w_1}\left[2\left(\frac{\partial w_3}{\partial x_2} - \frac{w_3}{w_1}\,\frac{\partial w_1}{\partial x_2}\right) - \left(\frac{\partial w_2}{\partial x_1} - \frac{w_2}{w_1}\,\frac{\partial w_1}{\partial x_1}\right)\right] \\ \frac{w_2}{w_1}\,\boldsymbol{R}_2^{(2)} + \frac{w_3}{w_1}\,\boldsymbol{R}_2^{(3)} + \frac{k}{c_v w_1}\Big[\frac{\partial w_4}{\partial x_1} - \frac{w_4}{w_1}\,\frac{\partial w_1}{\partial x_2} - \frac{1}{w_1}\left(w_2\,\frac{\partial w_2}{\partial x_2} + w_3\,\frac{\partial w_3}{\partial x_2}\right) \\ \qquad\qquad + \frac{1}{w_1^2}\,(w_2^2 + w_3^2)\,\frac{\partial w_1}{\partial x_2}\ \Big] \end{pmatrix},$$

where $\boldsymbol{R}_s^{(r)} = \boldsymbol{R}_s^{(r)}(\boldsymbol{w}, \nabla \boldsymbol{w})$ denotes the r-th component of $\boldsymbol{R}_s$ $(s = 1, 2,\ r = 2, 3)$.

Now for $\boldsymbol{w} = (w_1, \ldots, w_4)^{\mathrm{T}}$ and $\boldsymbol{\varphi} = (\varphi_1, \ldots, \varphi_4)^{\mathrm{T}}$ we define the vector-valued functions

$$\boldsymbol{D}_1(\boldsymbol{w}, \nabla \boldsymbol{w}, \boldsymbol{\varphi}, \nabla \boldsymbol{\varphi}) \tag{15}$$

$$= \begin{pmatrix} 0 \\ \frac{2}{3}\,\frac{\mu}{w_1}\left[2\left(\frac{\partial \varphi_2}{\partial x_1} - \frac{\varphi_2}{w_1}\,\frac{\partial w_1}{\partial x_1}\right) - \left(\frac{\partial \varphi_3}{\partial x_2} - \frac{\varphi_3}{w_1}\,\frac{\partial w_1}{\partial x_2}\right)\right] \\ \frac{\mu}{w_1}\left[\left(\frac{\partial \varphi_3}{\partial x_1} - \frac{\varphi_3}{w_1}\,\frac{\partial w_1}{\partial x_1}\right) + \left(\frac{\partial \varphi_2}{\partial x_2} - \frac{\varphi_2}{w_1}\,\frac{\partial w_1}{\partial x_2}\right)\right] \\ \frac{w_2}{w_1}\,\boldsymbol{D}_1^{(2)} + \frac{w_3}{w_1}\,\boldsymbol{D}_1^{(3)} + \frac{k}{c_v w_1}\Big[\frac{\partial \varphi_4}{\partial x_1} - \frac{\varphi_4}{w_1}\,\frac{\partial w_1}{\partial x_1} - \frac{1}{w_1}\left(w_2\,\frac{\partial \varphi_2}{\partial x_1} + w_3\,\frac{\partial \varphi_3}{\partial x_1}\right) \\ \qquad\qquad + \frac{1}{w_1^2}\,(w_2\varphi_2 + w_3\varphi_3)\,\frac{\partial w_1}{\partial x_1}\ \Big] \end{pmatrix},$$

$$\boldsymbol{D}_2(\boldsymbol{w}, \nabla \boldsymbol{w}, \boldsymbol{\varphi}, \nabla \boldsymbol{\varphi})$$

$$= \begin{pmatrix} 0 \\ \frac{\mu}{w_1}\left[\left(\frac{\partial \varphi_3}{\partial x_1} - \frac{\varphi_3}{w_1}\,\frac{\partial w_1}{\partial x_1}\right) + \left(\frac{\partial \varphi_2}{\partial x_2} - \frac{\varphi_2}{w_1}\,\frac{\partial w_1}{\partial x_2}\right)\right] \\ \frac{2}{3}\,\frac{\mu}{w_1}\left[2\left(\frac{\partial \varphi_3}{\partial x_2} - \frac{\varphi_2}{w_1}\,\frac{\partial w_1}{\partial x_2}\right) - \left(\frac{\partial \varphi_2}{\partial x_1} - \frac{\varphi_2}{w_1}\,\frac{\partial w_1}{\partial x_1}\right)\right] \\ \frac{w_2}{w_1}\,\boldsymbol{D}_2^{(2)} + \frac{w_3}{w_1}\,\boldsymbol{D}_2^{(3)} + \frac{k}{c_v w_1}\Big[\frac{\partial \varphi_4}{\partial x_2} - \frac{\varphi_4}{w_1}\,\frac{\partial w_1}{\partial x_2} - \frac{1}{w_1}\left(w_2\,\frac{\partial \varphi_2}{\partial x_2} + w_2\,\frac{\partial \varphi_3}{\partial x_2}\right) \\ \qquad\qquad + \frac{1}{w_1^2}\,(w_2\varphi_2 + w_3\varphi_2)\,\frac{\partial w_1}{\partial x_2}\ \Big] \end{pmatrix},$$

where $\boldsymbol{D}_s^{(r)}$ denotes the r-th component of $\boldsymbol{D}_s$ ($s = 1, 2,\ r = 2, 3$). Obviously, $\boldsymbol{D}_1$ and $\boldsymbol{D}_2$ are linear with respect to $\boldsymbol{\varphi}$ and $\nabla\boldsymbol{\varphi}$ and

$$\boldsymbol{D}_s(\boldsymbol{w}, \nabla\boldsymbol{w}, \boldsymbol{w}, \nabla\boldsymbol{w}) = \boldsymbol{R}_s(\boldsymbol{w}, \nabla\boldsymbol{w}), \quad s = 1, 2. \tag{16}$$

If $d = 3$, we proceed in a similar way.

Now, we define the diffusion form

$$\begin{aligned} a_h(\boldsymbol{w}, \boldsymbol{\varphi}) \;=\; & \sum_{i\in I} \int_{K_i} \sum_{s=1}^{d} \boldsymbol{R}_s(\boldsymbol{w}, \nabla\boldsymbol{w}) \cdot \frac{\partial \boldsymbol{\varphi}}{\partial x_s}\, dx \\ & - \sum_{i\in I} \sum_{\substack{j\in s(i)\\ j<i}} \int_{\Gamma_{ij}} \sum_{s=1}^{d} \langle \boldsymbol{R}_s(\boldsymbol{w}, \nabla\boldsymbol{w})\rangle\, (n_{ij})_s \cdot [\boldsymbol{\varphi}]\, dS \\ & + \sum_{i\in I} \sum_{\substack{j\in s(i)\\ j<i}} \int_{\Gamma_{ij}} \sum_{s=1}^{d} \langle \boldsymbol{D}_s(\boldsymbol{w}, \nabla\boldsymbol{w}, \boldsymbol{\varphi}, \nabla\boldsymbol{\varphi})\rangle\, (n_{ij})_s \cdot [\boldsymbol{w}]\, dS \\ & - \sum_{i\in I} \sum_{j\in\gamma_D(i)} \int_{\Gamma_{ij}} \sum_{s=1}^{d} \boldsymbol{R}_s(\boldsymbol{w}, \nabla\boldsymbol{w})\, (n_{ij})_s \cdot \boldsymbol{\varphi}\, dS \\ & + \sum_{i\in I} \sum_{j\in\gamma_D(i)} \int_{\Gamma_{ij}} \sum_{s=1}^{d} \boldsymbol{D}_s(\boldsymbol{w}, \nabla\boldsymbol{w}, \boldsymbol{\varphi}, \nabla\boldsymbol{\varphi})\, (n_{ij})_s\, \boldsymbol{w}\, dS, \end{aligned}$$

which is linear with respect to $\boldsymbol{\varphi}$ and $\nabla\boldsymbol{\varphi}$. Moreover, we introduce the forms:

$$(\boldsymbol{w}, \boldsymbol{\varphi}) = \int_{\Omega_h} \boldsymbol{w} \cdot \boldsymbol{\varphi}\, dx \tag{17}$$

($L^2(\Omega_h)$-scalar product),

$$J_h(\boldsymbol{w}, \boldsymbol{\varphi}) \;=\; \sum_{i\in I} \sum_{\substack{j\in s(i)\\ j<i}} \int_{\Gamma_{ij}} \sigma[\boldsymbol{w}] \cdot [\boldsymbol{\varphi}] dS + \sum_{i\in I} \sum_{j\in\gamma_D(i)} \int_{\Gamma_{ij}} \sigma\, \boldsymbol{w} \cdot \boldsymbol{\varphi}\, dS \tag{18}$$

(interior and boundary penalty jump terms),

$$\begin{aligned} \beta_h(\boldsymbol{w}, \boldsymbol{\varphi}) \;=\; & \sum_{i\in I} \sum_{j\in\gamma_D(i)} \int_{\Gamma_{ij}} \sum_{s=1}^{d} \boldsymbol{R}_s(\boldsymbol{w}, \nabla\boldsymbol{\varphi})\, (n_{ij})_s \cdot \boldsymbol{w}_B\, dS \\ & + \sum_{i\in I} \sum_{j\in\gamma_D(i)} \int_{\Gamma_{ij}} \sigma\, \boldsymbol{w}_B \cdot \boldsymbol{\varphi}\, dS \end{aligned}$$

(right-hand side form). We set $\sigma|_{\Gamma_{ij}} = \mu/d(\Gamma_{ij})$. The boundary state $\boldsymbol{w}_B$ is defined as

$$\begin{aligned} \boldsymbol{w}_B &= (\rho_{ij}, 0, \ldots, 0, \rho_{ij}\theta_{ij}) \quad \text{on } \Gamma_W, \\ \boldsymbol{w}_B &= \left(\rho_D, \rho_D v_{D1}, \ldots, \rho_D v_{Dd}, \rho_D\theta_D + \frac{1}{2}\rho_D |\boldsymbol{v}_D|^2\right) \quad \text{on } \Gamma_I, \end{aligned} \tag{19}$$

where ρ_D and $\boldsymbol{v}_D = (v_{D1}, \ldots, v_{Dd})$ are the given density and velocity from the boundary conditions (5) – (7) and ρ_{ij}, θ_{ij} are the values of the density and absolute temperature extrapolated from K_i onto Γ_{ij}.

The convective terms are represented by the form

$$b_h(\boldsymbol{w}_h, \boldsymbol{\varphi}_h) = -\sum_{i\in I} \int_{K_i} \sum_{s=1}^{d} \boldsymbol{f}_s(\boldsymbol{w}_h) \cdot \frac{\partial \boldsymbol{\varphi}_h}{\partial x_s}\, dx \tag{20}$$
$$+\sum_{i\in I} \sum_{j\in S(i)} \int_{\Gamma_{ij}} \boldsymbol{H}(\boldsymbol{w}_h|_{\Gamma_{ij}}, \boldsymbol{w}_h|_{\Gamma_{ji}}, \boldsymbol{n}_{ij}) \cdot \boldsymbol{\varphi}_h dS, \quad \boldsymbol{w}_h, \boldsymbol{\varphi}_h \in H^1(\Omega, \mathcal{T}_h)^m,$$

where H is a numerical flux (approximate Riemann solver) from the finite volume method. We assume that H is continuous, consistent and conservative, see [19] or [20]. If $\Gamma_{ij} \subset \partial\Omega_h$, then there is no neighbour K_j of K_i adjacent to Γ_{ij}. Then the values of $\boldsymbol{w}_h|_{\Gamma_{ij}}$ are determined on the basis of *"inviscid" boundary conditions*. We put $\boldsymbol{v} \cdot \boldsymbol{n} = 0$ on Γ_W and on Γ_I and Γ_O we consider the boundary conditions, which were derived for a linearized system of the 1D inviscid Euler equations. It means that we prescribe m_n components of $\boldsymbol{w}$, and the other components are extrapolated from interior of Ω. Here m_n is the number of negative eigenvalues of the Jacobi matrix

$$\sum_{s=1}^{N} \frac{D\boldsymbol{f}_s(\boldsymbol{w})}{D\boldsymbol{w}} n_s. \tag{21}$$

For more detail see [19], [20].

Now the *discrete DGFE Navier-Stokes problem* reads: An approximate DGFE solution of the compressible Navier-Stokes problem (CFP) is defined as a vector-valued function $\boldsymbol{w}_h$ such that

$$\text{a)} \quad \boldsymbol{w}_h \in C^1([0,T]; \boldsymbol{S}_h) \tag{22}$$
$$\text{b)} \quad \frac{\mathrm{d}}{dt}\left(\boldsymbol{w}_h(t), \boldsymbol{\varphi}_h\right) + b_h\left(\boldsymbol{w}_h(t), \boldsymbol{\varphi}_h\right) + a_h\left(\boldsymbol{w}_h(t), \boldsymbol{\varphi}_h\right) + J_h(\boldsymbol{w}, \boldsymbol{\varphi})$$
$$= \beta_h\left(\boldsymbol{w}_h(t), \boldsymbol{\varphi}_h\right) \qquad \forall\, \boldsymbol{\varphi}_h \in \boldsymbol{S}_h,\ t \in (0,T),$$
$$\text{c)} \quad \boldsymbol{w}_h(0) = \boldsymbol{w}_h^0,$$

where $\boldsymbol{w}_h^0$ is an $\boldsymbol{S}_h$-approximation of $\boldsymbol{w}^0$. Let us note that in the form a_h we apply the nonsymmetric variant of diffusion terms. In Section 4. we also consider the symmetric variant of the discretization for a scalar model equation.

Other formulations of the DGFE Navier-Stokes problem can be found in [2] and [4]. Various types of the DGFE approximations of diffusion terms (in the case of a scalar Poisson equation) are analyzed in [5].

Up to now we have approximated the domain Ω by a polygonal ($d = 2$) or polyhedral ($d = 3$) domain. In the case of a curved boundary $\partial\Omega$, superparametric finite elements have to be used, in order to get a numerical solution admissible from physical point of view – see [11]. For transonic flow, when the solution contains steep

gradients, the limiting of the order of the method explained in [17] is applied in order to avoid spurious unphysical overshoots and undershoots near steep gradients.

Problem (22) is equivalent to a large system of ordinary differential equations. Of course, in practical computations, suitable time discretization has to be applied. Here we use the forward Euler method, which is unfortunately conditionally stable and, thus, the time step has to be chosen very small. The extension of semi-implicit schemes from [12] to viscous flow is in progress.

3. Numerical examples

We present two cases of the DGFE solution of the viscous flow past the airfoil NACA0012 with the following data from [6]:

case	M_{in}	α	Re
C3	0.85	0°	500
C2	2.00	10°	106

Here M_{in} is the far field Mach number, α the angle of attack and Re the Reynolds number. The results correspond to the steady-state solution obtained by the time stabilization for $t \to \infty$. We compare our results with numerical simulations presented in [6], where ten methods were applied. Table 1 contains our computed lift c_L and drag c_R coefficients in comparison with [6] ($\#\mathcal{T}_h$ denotes the number of elements of the mesh $\mathcal{T}_h$).

		computed values		reference values from [6]	
case	$\#\mathcal{T}_h$	c_L	c_D	c_L	c_D
C3	4946	0.0003	0.2304	(0.0000 – 0.0007)	(0.1790 – 0.2420)
C2	5640	0.3969	0.4172	(0.3063 – 0.4059)	(0.4120 – 0.4910)

Tab. 1: *The computed values of drag and lift correspond to the reference values from [6].*

Figure 1 shows the Mach number isolines for the case C3. Figure 2 shows the triangulation and computed Mach number isolines for the case C2 with conspicuous shock wave (smeared due to the viscosity) and wake.

The isolines are not smooth in areas, where the mesh is coarse. On the other hand, we see that the quality of isolines is better in a neighbourhood of the profile, where the mesh was refined.

More examples and some further details can be found in [10].

4. Verification of the accuracy

Theoretical investigation of the accuracy of the DGFEM for the solution of the compressible Navier-Stokes equations is beyond the possibility of contemporary numerical analysis. Therefore, it is necessary (as is quite common in computational

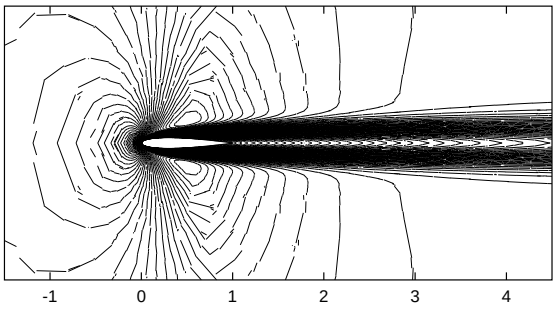

Fig. 1: *Viscous flow along NACA 0012, Mach number isolines for the case* C3.

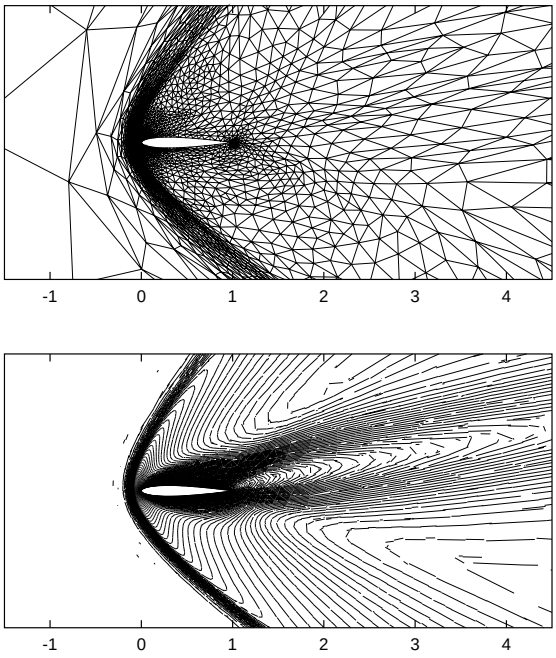

Fig. 2: *Viscous flow past NACA 0012, case* C2*, triangulation (top), Mach number isolines (bottom).*

fluid dynamics) to rely on the analysis of error estimates and numerical experiments carried out for simplified model problems.

In [21], error estimates of the DGFEM are obtained in the case of a linear initial-boundary value convection-diffusion-reaction problem. The $L^2(0,T;L^2(\Omega))$ – norm of the error is of the order $O(h^{p+1/2})$ uniformly with respect to the diffusion coefficient $\varepsilon \to 0+$.

Papers [18] and [13] are concerned with the error analysis of the space semidiscretization for nonstationary nonlinear convection-diffusion problems. In [14], the fully discretized nonstationary nonlinear convection-diffusion problem is analyzed. Due to the nonlinear convective terms, the error estimate in the $L^2(Q_T)$-norm is $O(h^p)$. Hence, it is not optimal.

Here we verify the order of convergence of the DGFEM with the aid of numerical experiments carried out for the DGFEM applied to the problem to find $u : Q_T = \Omega \times (0,T) \to I\!R$ such that

$$\begin{aligned} &\text{a)} \quad \frac{\partial u}{\partial t} + \sum_{s=1}^{d} \frac{\partial f_s(u)}{\partial x_s} = \varepsilon \Delta u + g \quad \text{in } Q_T, \\ &\text{b)} \quad u|_{\Gamma_D \times (0,T)} = u_D, \\ &\text{c)} \quad \varepsilon \frac{\partial u}{\partial n}|_{\Gamma_N \times (0,T)} = g_N, \\ &\text{d)} \quad u(x,0) = u^0(x), \quad x \in \Omega. \end{aligned} \tag{23}$$

We assume that $\Omega \subset I\!R^2$ is a bounded domain with a Lipschitz-continuous boundary $\partial\Omega = \Gamma_D \cup \Gamma_N$, $\Gamma_D \cap \Gamma_N = \emptyset$ and $T > 0$. The diffusion coefficient $\varepsilon > 0$ is a given constant, $g : Q_T \to I\!R$, $u_D : \Gamma_D \times (0,T) \to I\!R$, $g_N : \Gamma_N \times (0,T) \to I\!R$ and $u^0 : \Omega \to I\!R$ are given functions, $f_s \in C^1(I\!R)$, $s = 1, \ldots, d$, are given inviscid fluxes.

We consider two versions of the discretization of the diffusion terms:

$$\begin{aligned} a_h(u,\varphi) &= \sum_{i \in I} \int_{K_i} \varepsilon \, \nabla u \cdot \nabla \varphi \, dx \\ &- \sum_{i \in I} \sum_{\substack{j \in s(i) \\ j<i}} \int_{\Gamma_{ij}} \varepsilon \langle \nabla u \rangle \cdot \boldsymbol{n}_{ij} [\varphi] \, dS \mp \sum_{i \in I} \sum_{\substack{j \in s(i) \\ j<i}} \int_{\Gamma_{ij}} \varepsilon \langle \nabla \varphi \rangle \cdot \boldsymbol{n}_{ij} [u] \, dS \\ &- \sum_{i \in I} \sum_{j \in \gamma_D(i)} \int_{\Gamma_{ij}} \varepsilon \, \nabla u \cdot \boldsymbol{n}_{ij} \, \varphi \, dS \mp \sum_{i \in I} \sum_{j \in \gamma_D(i)} \int_{\Gamma_{ij}} \varepsilon \, \nabla \varphi \cdot \boldsymbol{n}_{ij} \, u \, dS \end{aligned} \tag{24}$$

(with the sign $-$ for symmetric variant and the sign $+$ for nonsymmetric variant of the diffusion form). Further, similarly as above, we introduce the form

$$J_h(u,\varphi) = \sum_{i \in I} \sum_{\substack{j \in s(i) \\ j<i}} \int_{\Gamma_{ij}} \sigma [u] \, [\varphi] \, dS + \sum_{i \in I} \sum_{j \in \gamma_D(i)} \int_{\Gamma_{ij}} \sigma \, u \, \varphi \, dS, \tag{25}$$

representing the interior and boundary penalty jump terms, and set

$$\begin{aligned} \ell_h(\varphi)(t) &= \int_\Omega g(t) \, \varphi \, dx + \sum_{i \in I} \sum_{j \in \gamma_N(i)} \int_{\Gamma_{ij}} g_N(t) \, \varphi \, dS \\ &\mp \sum_{i \in I} \sum_{j \in \gamma_D(i)} \int_{\Gamma_{ij}} \varepsilon \, \nabla \varphi \cdot \boldsymbol{n}_{ij} \, u_D(t) \, dS + \sum_{i \in I} \sum_{j \in \gamma_D(i)} \int_{\Gamma_{ij}} \sigma \, u_D(t) \, \varphi \, dS, \end{aligned} \tag{26}$$

where the sign $-$ is used for the symmetric variant of the right-hand side form and the sign $+$ gives the nonsymmetric right-hand side form. The weight σ is defined

as $\sigma|_{\Gamma_{ij}} = C\varepsilon/d(\Gamma_{ij})$, where C is a suitable constant ($C = 1$ for the nonsymmetric variant; for the symmetric variont, see [13]). Finally, the convective terms are approximated with the aid of a numerical flux $H = H(u, v, \boldsymbol{n})$ by the form

$$\begin{aligned} b_h(u,\varphi) &= -\sum_{i\in I}\int_K \sum_{s=1}^{d} f_s(u)\,\frac{\partial\varphi}{\partial x_s}\,dx \\ &\quad +\sum_{i\in I}\sum_{j\in S(i)} H\left(u|_{\Gamma_{ij}}, u|_{\Gamma_{ji}}, \boldsymbol{n}_{ij}\right)\varphi|_{\Gamma_{ij}}\,dS, \quad u,\,\varphi\in H^2(\Omega,\mathcal{T}_h). \end{aligned} \tag{27}$$

In the definition of the form b_h the following numerical flux is used

$$H(u_1,u_2,\boldsymbol{n}) = \begin{cases} \sum_{s=1}^{2} f_s(u_1)n_s, & \text{if } A>0 \\ \sum_{s=1}^{2} f_s(u_2)n_s, & \text{if } A\le 0 \end{cases}, \tag{28}$$

where

$$A = \sum_{s=1}^{2} f_s'(\bar u)n_s, \quad \bar u = \frac{1}{2}(u_1+u_2). \tag{29}$$

One can see that H is continuous, consistent and conservative. Of course, if $j\in\gamma(i)$ and $\Gamma_{ij}\subset\partial\Omega$, it is necessary to specify the meaning of $u|_{\Gamma_{ji}}$. Here we use the extrapolation, i. e. we set $u|_{\Gamma_{ji}} := u|_{\Gamma_{ij}}$.

Now both the symmetric and nonsymmetric *discrete problem* is formulated in the following way. Find an *approximate DGFE solution* u_h satisfying the following conditions:

$$\begin{aligned} &\text{a)} \quad u_h\in C^1([0,T];S_h), \\ &\text{b)} \quad \frac{d}{dt}(u_h(t),\varphi_h) + b_h(u_h(t),\varphi_h) + a_h(u_h(t),\varphi_h) + J_h(u_h(t),\varphi_h) \\ &\qquad\qquad = \ell_h(\varphi_h)(t) \qquad \forall\,\varphi_h\in S_h,\ \forall\, t\in(0,T), \\ &\text{c)} \quad u_h(0) = u_h^0, \end{aligned} \tag{30}$$

where u_h^0 is an S_h-approximation of the initial condition u^0.

In what follows we present numerical experiments comparing nonsymmetric and symmetric variants of the DGFEM applied to the 2D viscous Burgers equation

$$\frac{\partial u}{\partial t} + u\frac{\partial u}{\partial x_1} + u\frac{\partial u}{\partial x_2} = \varepsilon\Delta u + g, \quad \text{in } \Omega\times(0,T), \tag{31}$$

where $\Omega = (0,1)^2$, $\varepsilon = 0.002$. Dirichlet condition is prescribed on the whole boundary $\partial\Omega$. We define the functions u_D, u^0 and g so that the exact solution has the form

$$u(x_1,x_2,t) = \left(1-e^{-t}\right)\left(x_1x_2^2 - x_2^2e^{2\frac{x_1-1}{\nu}} - x_1e^{3\frac{x_2-1}{\nu}} + e^{\frac{2x_1+3x_2-5}{\nu}}\right), \tag{32}$$

where $\nu>0$ is a given number. In order to investigate the asymptotic behaviour of the error with respect to time, we seek the steady-state solution

$$u^{\mathrm{st}}(x_1,x_2) = \lim_{t\to\infty} u(x_1,x_2,t) = x_1x_2^2 - x_2^2e^{2\frac{x_1-1}{\nu}} - x_1e^{3\frac{x_2-1}{\nu}} + e^{\frac{2x_1+3x_2-5}{\nu}} \tag{33}$$

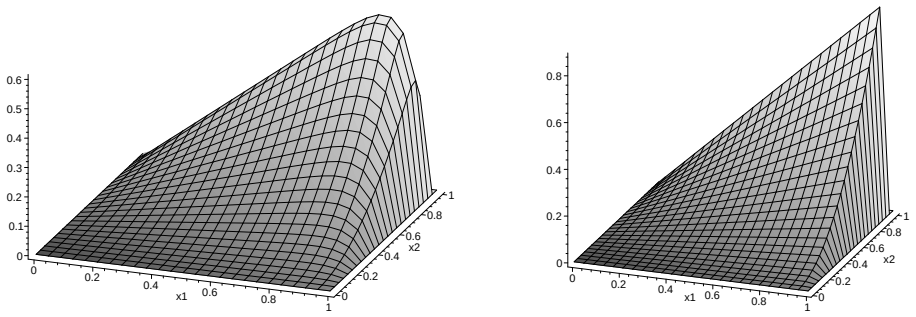

Fig. 3: *The steady-state solution (33) for* $\nu = 0.1$ *(left) and* $\nu = 0.01$ *(right).*

by the time stabilization method, i. e. we solve the problem (31) for "$t \to \infty$". The function (33) has two "boundary layers" along the edges $\{(1, x_2);\ x_2 \in (0,1)\}$ and $\{(x_1, 1);\ x_1 \in (0,1)\}$. The steepness is given by the parameter ν. The experiments were performed with piecewise linear elements (i.e. $p = 1$) for $\nu = 0.1$ and $\nu = 0.01$, see Figure 3 showing the exact steady-state solutions. The resulting system of ODE's equivalent with scheme (30) is solved by the forward Euler method with a small time step $\tau = 10^{-4}$, which guarantees stability and sufficiently precise resolution with respect to time.

The computational error of the steady-state solution is evaluated over the domain Ω in the $L^2(\Omega)-$ norm:

$$e_h \equiv \|u_h^{\mathrm{st}} - u^{\mathrm{st}}\|_{L^2(\Omega)}, \tag{34}$$

where u_h^{st} is the numerical solution obtained by the DGFEM and u^{st} is given by (33). We suppose that the error e_h behaves according to the formula

$$e_h \approx Ch^{\alpha}, \tag{35}$$

where $C > 0$ is a constant not depending on h and α is the *order of accuracy* of the method. The numerical solution was computed for 6 unstructured meshes ($\mathcal{T}_{h_l},\ l = 1, \ldots, 6$) with different h_l. We define the *local experimental order of convergence* by

$$\alpha_l = \frac{\log\left(e_{h_l}/e_{h_{l-1}}\right)}{\log\left(\tilde{h}_l/\tilde{h}_{l-1}\right)}, \quad l = 2, \ldots, 6. \tag{36}$$

Moreover, we define the *global experimental order of convergence* $\bar{\alpha}$ by the least squares method. By $\#\mathcal{T}_{h_l}$ we denote the number of elements and $\tilde{h}_l$ denotes the average diameter of elements from $\mathcal{T}_{h_l}$.

Tables 2 and 3 show the $L^2(\Omega)-$norm of the error e_{h_l} and the values of $\alpha_l,\ l = 2, \ldots, 6$, and $\bar{\alpha}$ for the parameters $\nu = 0.1$ and $\nu = 0.01$, respectively. Figures 4 and 5 show the computed numerical results on the mesh $\mathcal{T}_{h_6}$. We see that the numerical solution is continuous although the discontinuous approximation is used.

			symmetric DGFEM		nonsymmetric DGFEM	
l	$\#\mathcal{T}_{h_l}$	h_l	e_h	α_l	e_h	α_l
1	148	1.265E-01	3.2192E-02	–	2.6097E-02	–
2	289	9.069E-02	1.8965E-02	1.590	1.4063E-02	1.858
3	591	6.323E-02	8.4306E-03	2.248	5.5749E-03	2.565
4	1056	4.730E-02	4.5989E-03	2.089	3.6166E-03	1.491
5	2360	3.151E-02	1.60598-03	2.589	1.7105E-03	1.842
6	4219	2.366E-02	1.3785E-03	0.532	1.4222E-03	0.643
global order of accuracy $\bar{\alpha}$				2.012		1.802

Tab. 2: *Computational errors in $L^2(\Omega)-$norm, the values of α_l, $l = 2, \ldots, 6$, and $\bar{\alpha}$ for $\nu = 0.1$.*

			symmetric DGFEM		nonsymmetric DGFEM	
l	$\#\mathcal{T}_{h_l}$	h_l	e_h	α_l	e_h	α_l
1	148	1.265E-01	no conver	–	6.6610E-01	–
2	289	9.069E-02	4.3996E-01	–	3.7808E-01	1.702
3	591	6.323E-02	1.0517E-01	3.968	9.1777E-02	3.925
4	1056	4.730E-02	6.7525E-02	1.527	5.8026E-02	1.580
5	2360	3.151E-02	2.98088-02	2.012	2.4281E-02	2.144
6	4219	2.366E-02	1.7649E-02	1.828	1.4895E-02	1.705
global order of accuracy $\bar{\alpha}$				2.278		2.342

Tab. 3: *Computational errors in $L^2(\Omega)-$norm, the values of α_l, $l = 2, \ldots, 6$, and $\bar{\alpha}$ for $\nu = 0.01$.*

Both (nonsymmetric as well as symmetric) variants of the DGFEM produce comparable results. They show that the experimental order of convergence is equal to two for a piecewise linear approximation. This means that theoretical error estimates are suboptimal. The derivation of optimal error estimates for the case of nonlinear problems is a difficult, but challenging task.

From Figure 5 we see that for $\nu = 0.01$ the approximate solutions suffer from the Gibbs phenomenon, manifested by undershoots and overshoots in boundary layers, but the order of accuracy is not decreased. The Gibbs phenomenon can be avoided by a suitable limiting of the order of accuracy of the space discretization in a vicinity of a steep gradient. See, [17].

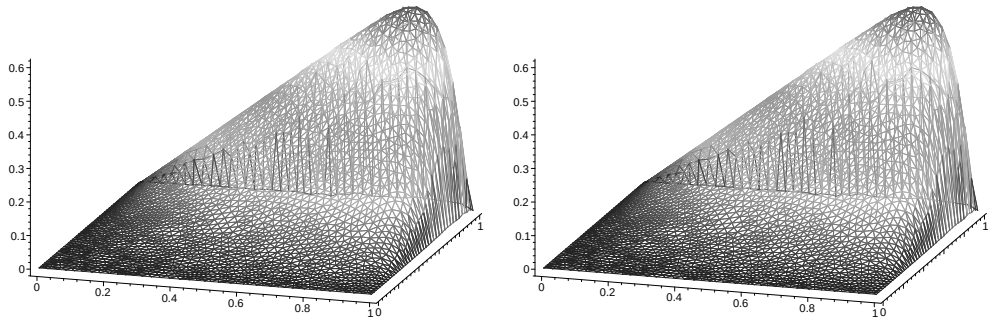

Fig. 4: *Numerical solution computed on $\mathcal{T}_{h_6}$ for $\nu = 0.1$, symmetric variant of DGFEM (left) and nosymmetric variant of DGFEM (right).*

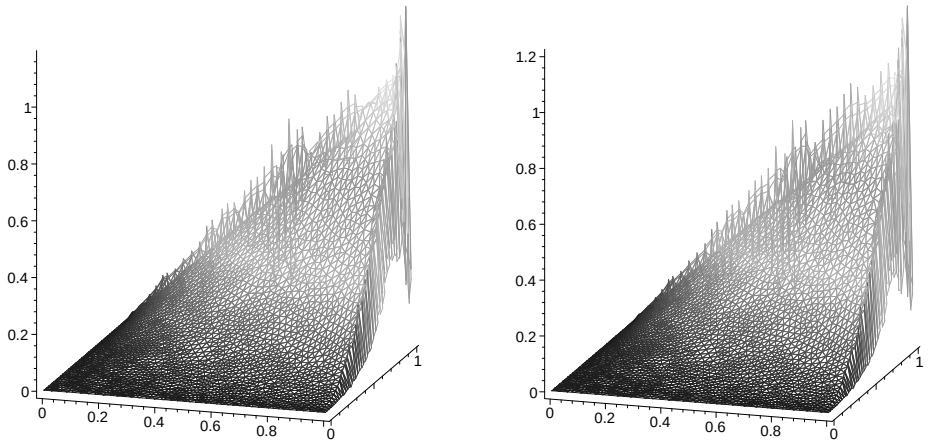

Fig. 5: *Numerical solution computed on $\mathcal{T}_{h_6}$ for $\nu = 0.01$, symmetric variant of DGFEM (left) and nosymmetric variant of DGFEM (right).*

References

[1] S. Adjerid, D. Devine, J.E. Flaherty, L. Krivodonova: *A posteriori error estimation for discontinuous Galerkin solutions of hyperbolic problems.* Comput. Methods Appl. Mech. Engrg. **191**, 2002, 1097–1112.

[2] F. Bassi, S. Rebay: *A high-order accurate discontinuous finite element method for the numerical solution of the compressible Navier–Stokes equations.* J. Comput. Phys., **131**, 1997, 267–279.

[3] F. Bassi, S. Rebay: *High-order accurate discontinuous finite element solution of the 2D Euler equations.* J. Comput. Phys., **138**, 1997, 251–285.

[4] C.E. Baumann, J.T. Tinsley: *A discontinuous hp finite element method for the Euler and Navier-Stokes equations.* Int. J. Numer. Methods Fluids, **31**, 1999, 79–95.

[5] F. Brezzi, G. Manzini, D. Marini, P. Pietra, A. Russo: *Discontinuous Galerkin approximations for elliptic problems.* Numer. Methods Partial Differ. Equations, **16**, 2000, 365–378.

[6] M.O. Bristeau, R. Glowinski, J. Periaux, H. Viviand (Eds.): *Numerical Simulation of Compressible Navier-Stokes Flows.* Notes on Numerical Fluid Mechanics, Volume 18, Vieweg, Braunschweig, 1987.

[7] B. Cockburn: *Discontinuous Galerkin methods for convection dominated problems.* In T. J. Barth and H. Deconinck (Eds.) High–Order Methods for Computational Physics, Lecture Notes in Computational Science and Engineering 9, Berlin, Springer-Verlag 1999, 69–224.

[8] B. Cockburn, G.E. Karniadakis, C.-W. Shu (Eds.): *Discontinuous Galerkin methods.* Lecture Notes in Computational Science and Engineering 11, Berlin, Springer-Verlag, 2000.

[9] B. Cockburn, C.W. Shu: *TVB Runge–Kutta local projection discontinuous Galerkin finite element for conservation laws II: General framework.* Math. Comput. **52**, 1989, 411–435.

[10] V. Dolejší: *On the discontinuous Galerkin method for the numerical solution of the Euler and the Navier-Stokes equations.* Int. J. Numer. Methods Fluids (to appear).

[11] V. Dolejší, M. Feistauer: *On the discontinuous Galerkin method for the numerical solution of compressible high-speed flow.* In: F. Brezzi, A. Buffa, S. Corsaro, A. Murli (Eds.), Numerical Mathematics and Advanced Applications, ENUMATH 2001, Milano, Springer-Verlag Italia, 2003, 65–84.

[12] V. Dolejší, M. Feistauer: *A semi-implicit discontinuous Galerkin finite element method for the numerical solution of inviscid compressible flow.* J. Comput. Phys., **198**, 2004, 727–746.

[13] V. Dolejší, M. Feistauer: *Error estimates of the discontinuous Galerkin method for nonlinear nonstationary convection-diffusion problems.* Numer. Funct. Anal. Optimiz. (submitted).

[14] V. Dolejší, M. Feistauer: *Analysis of semi-implicit DGFEM for nonlinear convection-diffusion problems.* Numer. Math. (submitted).

[15] V. Dolejší, M. Feistauer, C. Schwab: *A finite volume discontinuous Galerkin scheme for nonlinear convection–diffusion problems.* Calcolo **39**, 2002, 1–40.

[16] V. Dolejší, M. Feistauer, C. Schwab: *On discontinuous Galerkin methods for nonlinear convection–diffusion problems and compressible flow.* Mathematica Bohemica **127**, 2002, 163–179.

[17] V. Dolejší, M. Feistauer, C. Schwab: *On some aspects of the discontinuous Galerkin finite element method for conservation laws.* Math. Comput. Simul. **61**, 2003, 333–346.

[18] V. Dolejší, M. Feistauer, V. Sobotíková: *Analysis of the discontinuous Galerkin method for nonlinear convection–diffusion problems.* Comput. Methods Appl. Mech. Engrg. (submitted).

[19] M. Feistauer: *Mathematical methods in fluid dynamics.* Harlow, Longman Scientific & Technical, 1993.

[20] M. Feistauer, J. Felcman, I. Straškraba: *Mathematical and computational methods for compressible flow.* Oxford, Clarendon Press, 2003.

[21] M. Feistauer, K. Švadlenka: *Discontinuous Galerkin method of lines for solving nonstationary singularly perturbed linear problems.* J. Numer. Math. **12**, 2004, 97–117.

[22] R. Hartmann, P. Houston: *Adaptive discontinuous Galerkin finite element methods for nonlinear hyperbolic conservation laws.* SIAM J. Sci. Comp., **24**, 2002, 979–1004.

[23] R. Hartmann, P. Houston: *Adaptive discontinuous Galerkin finite element methods for the compressible Euler equations.* J. Comput. Phys., **183**, 2002, 508–532.